Improving Wet Refractivity Estimation via GNSS Tropospheric Tomography: A Case Study in the Northwest and North of Iran

Arash Tayfehrostami *, Yazdan Amerian, Saeed Izanlou

Faculty of Geodesy and Geomatics Engineering, K. N. Toosi University of Technology, Tehran, Iran
a.tayfehrostami@email.kntu.ac.ir; amerian@kntu.ac.ir; saeed.izanlo@email.kntu.ac.ir

KEY WORDS: Global Navigation Satellite Systems, Wet Refractivity, Tomography, Troposphere, Zenith Wet Delay, Radiosonde.

ABSTRACT:

Water vapor plays a critical role in atmospheric processes, yet its dynamic nature poses challenges for accurate measurement. Traditional methods like radiosondes lack sufficient spatial and temporal resolution, prompting the use of Global Navigation Satellite Systems (GNSS) tomography for improved wet refractivity estimation. This study investigates the feasibility of GNSS tomography in northern and northwest Iran, leveraging data from 20 GNSS stations and radiosonde measurements from Tabriz and Tehran. A voxel-based tomographic model was employed, with horizontal resolutions of 0.37°–0.5° and vertical resolutions of 500–1000 m. The results were validated against radiosonde data, revealing Root Mean Square Error (RMSE) values ranging from 1.58 to 2.91 ppm in Tabriz and 2.02 to 2.16 ppm in Tehran. These findings demonstrate the potential of GNSS tomography to complement traditional methods, particularly in regions with sparse observational networks. The study highlights the importance of optimal voxel resolution and geometric constraints in enhancing tomographic accuracy, offering a promising approach for regional weather monitoring and climate research.

1. INTRODUCTION

Water vapor plays a fundamental role in the key physical and chemical processes of the atmosphere, and its spatial and temporal variability exerts a significant influence on weather patterns (Jacob, 2001; Turco, 1992). Within the troposphere, water vapor is a highly dynamic component, with concentrations capable of varying by several orders of magnitude over distances of less than 10 kilometres (Couvreux et al., 2005). Due to this inherent variability, obtaining high-resolution measurements of water vapor distribution is critical for accurate weather forecasting (Stensrud, 2009). Traditional measurement methods, such as those relying on radiosonde stations, are limited by their coarse spatial and temporal resolution (e.g., every 12 hours and spaced 250 kilometres apart in Europe (Guerova et al., 2016), which fails to adequately capture the rapid dynamics of humidity changes. To address this limitation, a new observational system has been developed, leveraging data from the Global Navigation Satellite Systems (GNSS).

When GNSS signals traverse the atmosphere, they are influenced by various effects arising from the distinct characteristics of atmospheric layers. Among these, the troposphere is particularly significant in transmitting GNSS signals to ground-based receivers. This layer causes a bending effect on the satellite signal paths due to the propagation behaviour of electromagnetic waves. Furthermore, the refractive index of the troposphere is susceptible to temperature, pressure, and water vapor content, reflecting its physical properties. As a result, modeling the refractive index—especially the wet component of the troposphere—is complex, given the dynamic and rapidly changing conditions within this layer (Seeber, 2003). As a result, the tropospheric error in GNSS signals can be utilized as a valuable data source for meteorological studies, allowing for the estimation of parameters such as Integrated Water Vapor (IWV) or Precipitable Water Vapor (PWV) (Bevis et al., 1992).

In recent years, GNSS tomography has become one of the most promising methods for reconstructing the spatial and temporal structure of the troposphere. This technique involves defining a three-dimensional (3D) grid that spans both horizontally and vertically, extending from the ground-based GNSS network to an effective height within the troposphere.

In recent years, an increasing number of studies have highlighted the potential of GNSS tomography for reconstructing the three-dimensional structure of the troposphere (Bender et al., 2011; Benevides et al., 2018; Flores, LP, et al., 2000; Flores, Ruffini, et al., 2000; Guo et al., 2016; Heublein et al., 2019; Nilsson & Elgered, 2007; Rohm & Bosy, 2009; Trzcina & Rohm, 2019). Furthermore, various countries have developed tomographic models to estimate 3D wet refractivity or water vapor fields by utilizing moderately dense GNSS networks (Brenot et al., 2018; Champollion et al., 2005; de Sá, 2019; Forootan et al., 2021, 2023; Haji-Aghajany, 2021; Möller, 2017; Rohm et al., 2014). To evaluate the accuracy and reliability of these tomographic reconstructions, independent data sources such as radiosonde measurements, Water Vapor Radiometers (WVR), and numerical weather prediction models have been used (Bastin et al., 2007; Brenot et al., 2018; Elgered et al., 1991; Gradinarsky & Jarlemark, 2004; Hanna et al., 2019; Nilsson & Elgered, 2007; Notarpietro et al., 2011; Troller, 2004; Van Baelen et al., 2011). Recently, Haji-Aghajany et al. (2025) introduced an explainable deep learning-based downscaling framework for high-resolution voxel-based GNSS tropospheric tomography, which significantly enhances spatial detail and retrieval accuracy. This novel approach provides physically interpretable reconstructions of fine-scale atmospheric structures (Haji-Aghajany et al., 2025). Despite these advancements, challenges remain in accurately reconstructing the wet component of the troposphere. Key issues include the uneven and insufficient distribution of

* Corresponding author

observations, which is closely tied to the geometric arrangement of GNSS satellites and receivers, the regularization techniques applied, and the selection of the a priori field. To date, the accuracy of reconstructed fields has been evaluated using ground-based GNSS observations (Haji-Aghajany et al., 2020, 2021, 2022; Haji-Aghajany & Amerian, 2018; Möller, 2017).

In this study, we present a feasibility analysis for implementing GNSS tomography in northern Iran, where the region's pronounced topographic variations pose unique challenges and opportunities. The spatial distribution of GNSS rays within the tomographic domain is carefully examined to determine the optimal placement of nodes, ensuring that the resolution matrix adequately captures the heterogeneity of the area. This investigation marks the first attempt to assess the applicability of tomographic techniques in northern Iran, complementing earlier studies conducted in the southwest. To validate our findings, radiosonde measurements are utilized as a reliable reference, providing an independent assessment of the reconstructed atmospheric fields.

2. CASE STUDY AND DATA

2.1 Case study

Iran, as a geographically expansive country, exhibits a wide range of climates and experiences diverse climatic phenomena, including heavy rainfall in the northern regions and severe tornadoes in the southern areas. This climatic variability is evident in the significant differences in annual precipitation, with some southern cities receiving less than 40 mm of rainfall, while western regions report over 600 mm. Additionally, the lack of comprehensive data and an organized data collection system creates significant challenges for assimilating numerical weather models with regional observations in Iran. For instance, there are only 14 radiosonde stations across the country, which are unevenly distributed and often do not operate on a regular schedule, limiting their effectiveness in weather forecasting and climate monitoring. To address these limitations, the application of tomographic methods offers a promising solution. By leveraging permanent GNSS stations and tomographic models, it is possible to establish a robust weather monitoring system tailored to each region of the country. Such a system could not only enhance the accuracy of weather predictions but also improve positioning precision, benefiting both meteorological studies and practical applications. This approach highlights the potential of GNSS-based technologies to compensate for the deficiencies in traditional observation networks and contribute to more reliable climate monitoring in Iran.

2.2 Data

2.2.1 GNSS Stations

In 2004, the Iran National Cartographic Center (https://ncc.gov.ir/) embarked on the development of a network known as the Iranian Permanent GPS Network (IPGN). This initiative was part of its broader efforts to investigate and mitigate earthquake-related risks in Iran. As a highly ambitious and valuable project, it marks a significant advancement in understanding tectonic deformation and reducing the impact of natural disasters, while simultaneously enhancing the country's scientific infrastructure. The design and implementation of this project have been enriched by contributions from academic and research institutions in France, the Geological Survey of Iran, and the International Institute of Earthquake Engineering and Seismology.

In this study, data were collected from 20 IPGN stations located in northern and north-western Iran. GNSS measurements were analyzed over three days, spanning from Day of Year (DOY) 295 to DOY 297 in 2022. Meteorological reports indicate that the humidity levels in the study area peak during this timeframe. It is important to note that some stations provided observations for only a limited number of days within this interval. The geodetic heights of the IPGN GNSS stations range from -20 meters to 2,513 meters above sea level.

2.2.2 Radiosonde

The study utilizes two radiosonde stations located near the cities of Tabriz and Tehran. In Tabriz, radiosonde balloons are launched once daily, while in Tehran, they are launched twice daily. Consequently, the accuracy of the calculated N_w from GNSS tomography can only be assessed during the specific epochs corresponding to the recorded radiosonde profiles. Table (1) shows the specifications of these sites.

Station name (Based on IATA airport code)	Latitude (°)	Longitude (°)	height (m)
TBZ	38.0833	46.2833	1367
THR	35.6833	51.3167	1204

Table 1. Specifications of radiosonde sites.

3. METHODS

The tomographic reconstruction of wet refractivity is initially presented as the foundational challenge in this study. Subsequently, the principles and practical implementations of voxel-based tomographic methodologies are elaborated. To establish the ideal dimensions for model elements, the resolution matrix is systematically employed as an analytical tool. It is noteworthy that tropospheric tomography inherently constitutes a highly ill-posed inverse problem, exacerbated by the integration of extensive observational datasets and the expansive nature of the modeling domain. Consequently, the adoption of regularization techniques becomes indispensable to ensure numerical stability and solution reliability.

3.1 GNSS tropospheric tomographic modeling

Slant Wet Delay (SWD), defined as the additional signal propagation delay caused by atmospheric water vapor along the slant path between a satellite and a receiver, constitutes a fundamental input parameter for tomographic reconstruction models (Haji-Aghajany et al., 2020):

$$SWD = 10^{-6} \int_{Rec.}^{Sat.} N_w \, ds \tag{1}$$

where s denotes the length of the ray and N_w represents the wet refractivity value. The SWD of the signal path is determined via the approach outlined by Davis et al. (1993), expressed as:

$$SWD = \left(mf_{wet} \times ZWD\right) + \left(mf_{wet} \times cot\left(\alpha\right) \times \left(\left(G_{NS}^{W} \times cos\,\alpha z\right) + \left(G_{EW}^{W} \times sin\,\alpha z\right)\right)\right) + R \tag{2}$$

Where G^{W}_{NS} *and* G^{W}_{WE} denote non-hydrostatic delay gradients along the north-south (N-S) and east-west (E-W) axes, respectively, while mf_{wet} represents the non-hydrostatic wet mapping function. The variables a (satellite elevation angle) and az (azimuth angle) are incorporated into this framework. The Zenith Wet Delay (ZWD) is derived by subtracting the Zenith

Hydrostatic Delay (ZHD) from the Zenith Total Delay (ZTD) (Izanlou et al., 2023; Tayfehrostami & Amerian, 2025).

In this study, the PRIDE PPP-AR software suite was employed to compute ZWD values. PRIDE PPP-AR, an open-source platform developed by the GNSS Research Center at Wuhan University, represents a state-of-the-art implementation of Precise Point Positioning (PPP) with ambiguity resolution capabilities. This software is renowned for its robust algorithms in processing GNSS data, enabling high-precision estimation of tropospheric delays like ZHD and ZWD, directly (Geng et al., 2019). Its integration of advanced stochastic models and real-time ionospheric corrections has solidified its position as a critical tool in geodetic and atmospheric research (Huang et al., 2019). In the following, the theories related to voxel-based tomography are explained.

Eq. (1) is applicable to continuous spatial problems, voxel-based tomography operates within a discrete space, which is divided into 3-D voxels, within which the N_w is assumed to remain constant over a defined time interval. Consequently, the relationship between the SWD and the N_w can be expressed in a discretized form as follows (Izanlou et al., 2024):

$$SWD^{i} = 10^{-6} \sum_{j=1}^{n} N_{wj} \Delta s_{j}^{i} \tag{3}$$

Where i represents the index of the GNSS ray, j denotes the voxel index, Δs^i_j signifies the length traversed by ray i within voxel j, and N_{wj} corresponds to the wet refractivity value within voxel j. Eq. (3) can be expressed in matrix form as follows:

$$_{T}L_{1} = {}_{T}A_{n\times m\times q\ n\times m\times q} N_{w} \tag{4}$$

Where, T represents the number of GNSS rays, A denotes the coefficient matrix, and N_w is the vector of unknown N_w values. To estimate the unknown parameters, an inversion algorithm must be employed. As noted earlier, in voxel-based tomography, the coefficient matrix is typically large and sparse, making it impossible to estimate all unknowns directly. Consequently, incorporating constraints through various methods becomes essential to address this limitation (Haji-Aghajany et al., 2022). However, the relatively limited accuracy of these constraints presents a notable challenge in improving the quality of tomographic outcomes. In this study, horizontal constraints are applied under the assumption that the N_w within a voxel is equivalent to the mean value of its horizontally neighboring voxels (Yao & Zhao, 2017). For vertical constraints, a negative exponential function is employed (Elósegui et al., 1998; Flores, Ruffini, et al., 2000):

$$N_{w\,i-1} = \nu_{i-1} N_{w\,i} \tag{5}$$

In Eq. (5), $\nu_{i-1} = e^{\left(\frac{h_{i-1}-h_i}{H}\right)}$ represents the coefficient between two consecutive layers, and h height in layers i-1 and i, and H is the water vapor scale height, which is empirically 1–2 km. The model resolution matrix is used to determine the optimal resolution and geometry for the tomography model.

Tropospheric tomography represents a large-scale, ill-posed inverse problem due to the extensive number of observations and the broad spatial coverage involved in modeling. Consequently, the application of regularization methods becomes essential to address this challenge. In this study, we employ the Simultaneous Algebraic Reconstruction Technique (SART) as a regularization method (Izanlou et al., 2024). Fig. 1 and Fig. 2 show the distribution of GNSS stations, radiosonde sites, and the horizontal structure of the voxels in the study regions.

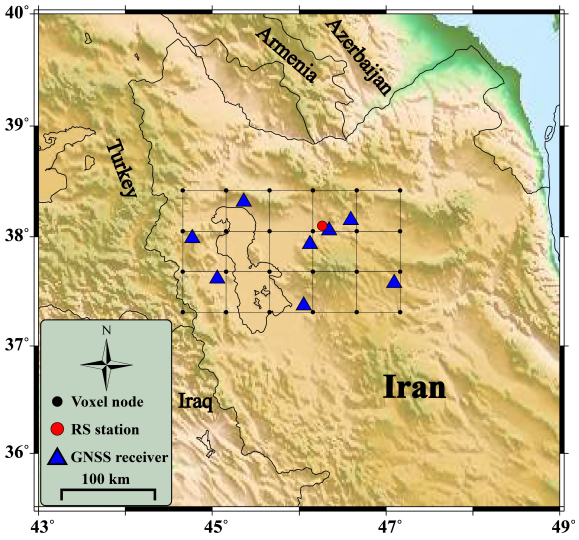

Figure 1. Distribution of GNSS stations, radiosonde site, and the horizontal layout of the voxels in the northwest region of Iran.

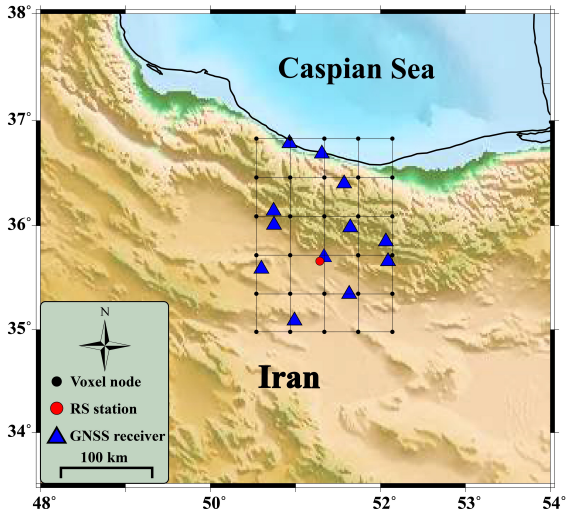

Figure 2. Distribution of GNSS stations, radiosonde site, and the horizontal structure of the voxels in the northern region of Iran.

4. RESULTS

This section presents an evaluation of the GNSS tomography results using radiosonde data. It is important to note that, considering the Tabriz radiosonde site collects data only once daily at 12:00 UTC, and the Tehran radiosonde site records data twice daily at 00:00 and 12:00 UTC, the comparison of N_w values for the DOYs 295, 296, and 297 was conducted at 12:00 UTC for both sites. Additionally, the results of the comparison are reported in tabular form, utilizing the Root Mean Square Error (RMSE) statistical metric.

4.1 Comparison of N_w obtained from GNSS tomography and RS in the northwest of Iran

The framework utilized for tomographic processing is illustrated in Fig. 3. Consistent with prior research outcomes, the most suitable horizontal resolution for the voxel-based tomography model was determined through an analysis of the resolution matrix. This matrix, which constitutes a critical element of the coefficient matrix, encapsulates both the resolution and geometric characteristics of the tomography model. It is worth noting that any negligible diagonal elements within this matrix can negatively affect the precision of parameter estimation. Efforts to optimize the design of the tomography model have resulted in a resolution matrix that closely resembles the identity matrix. For the tomography of this region, the resolution was 0.37° in the latitude direction and 0.5° in the longitude direction. The minimum latitude was 37.31°, with a maximum of 38.42°, while the minimum longitude was 44.66°, extending up to a maximum of 47.16°. Additionally, the vertical resolution is defined as 500 m for the first six layers, increasing to 1000 m for the subsequent seven layers.

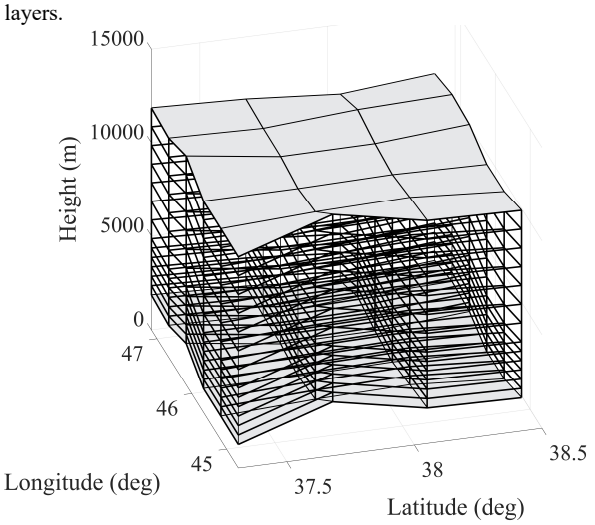

Figure 3. 3-D schematic of the tomography model.

Fig. 4 illustrates the comparative results of N_w values estimated through GNSS tomography and radiosonde measurements. This analysis focuses on the specific times of 12:00 UTC for the three consecutive days corresponding to DOYs 295, 296, and 297 in the year 2022. The figure highlights the consistency, discrepancies, and overall performance of the two methods in estimating Nw during these selected intervals. By examining the outcomes at these precise temporal points, the evaluation aims to provide insights into the reliability and accuracy of GNSS tomography in comparison to radiosonde data, which serves as a well-established reference in atmospheric studies.

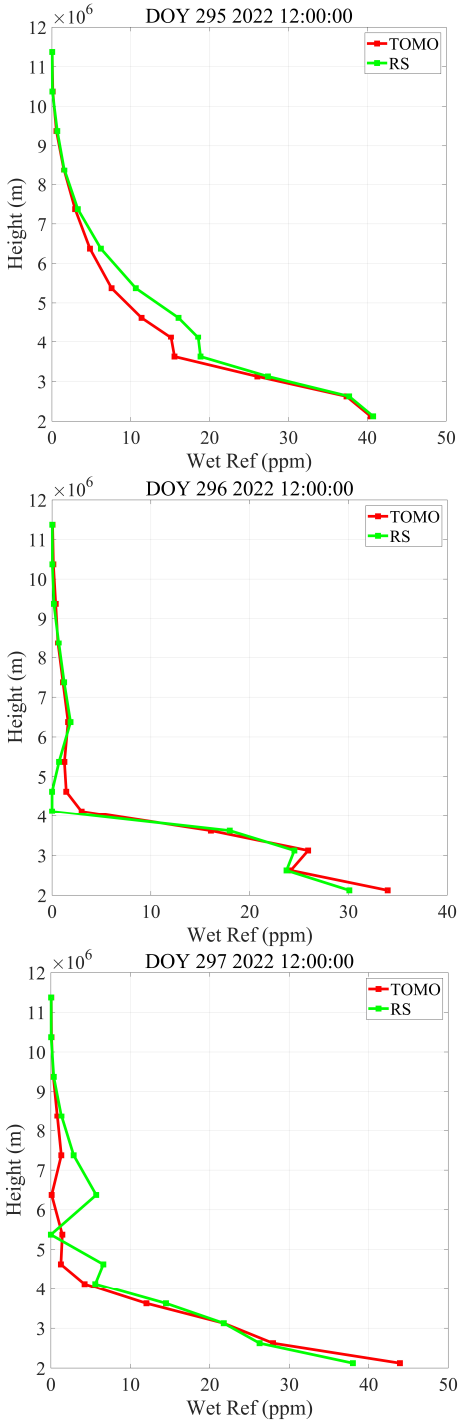

Figure 4. Comparison between GNSS tomography and RS in the Tabriz radiosonde site.

Table 2 presents the outcomes of the comparison using the RMSE metric. This statistical parameter serves as a key indicator for assessing the discrepancies between the estimated N_w values derived from GNSS tomography and those obtained through radiosonde measurements. By quantifying the differences between the two datasets, the RMSE provides a robust measure of the accuracy and reliability of the GNSS tomography model in replicating the radiosonde observations. The inclusion of this metric facilitates a more comprehensive

evaluation of the performance and precision of the tomographic approach under analysis.

DOY	RMSE (ppm)
295 12:00:00	2.12
296 12:00:00	1.58
297 12:00:00	2.91

Table 2. Comparison of N_w estimations from GNSS tomography and radiosonde using RMSE metric in the Tabriz radiosonde site.

4.2 Comparison of N_w obtained from GNSS tomography and RS in the north of Iran

Similar to the explanation given in Sec. 4.1 for northwest Iran, the tomographic processing for northern Iran was also performed similarly. For this region, the tomography was performed with a resolution of 0.37° in the latitude direction and 0.4° in the longitude direction. The minimum latitude was 34.98°, with a maximum of 36.83°, while the minimum longitude was 50.54°, extending up to a maximum of 52.14°. Fig. 5 shows the 3-D skeleton of the tomography model for this region.

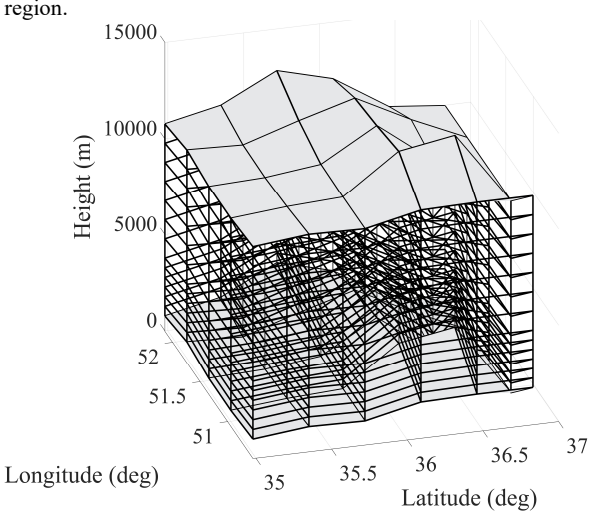

Fig. 5. 3-D schematic of the tomography model.

Fig. 6 show the comparative analysis of N_w values estimated using GNSS tomography and radiosonde measurements at 12:00 UTC for DOY 295, 296, and 297, respectively.

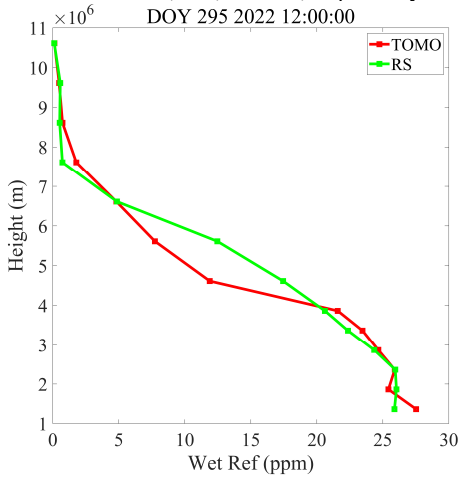

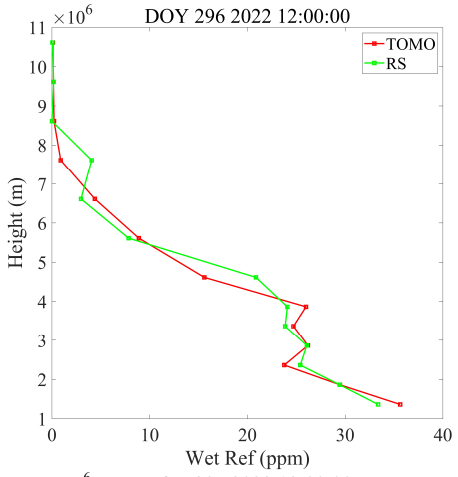

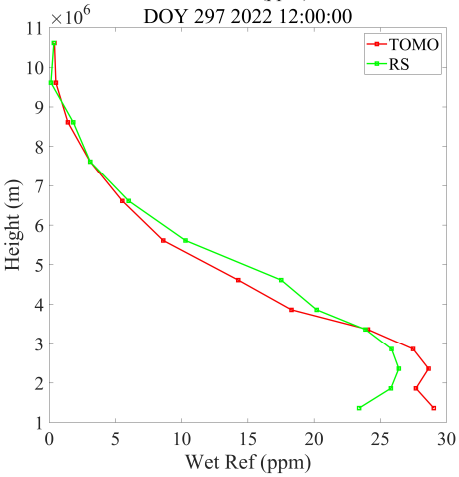

Fig. 6. Comparison between GNSS tomography and RS in the Tehran radiosonde site in 12 UTC.

Table 3 shows the outcomes of the comparison using the RMSE metric.

DOY	RMSE (ppm)
295 12:00:00	2.14
296 12:00:00	2.02
297 12:00:00	2.16

Table 3. Comparison of N_w estimations from GNSS tomography and radiosonde using RMSE metric in the Tehran radiosonde site.

5. CONCLUSION

This study evaluated the performance of GNSS tomography for estimating wet refractivity in northern and northwest Iran, addressing the limitations of traditional radiosonde measurements. By analyzing data from 20 GNSS stations and validating results against radiosonde observations, the research demonstrated the effectiveness of tomographic techniques in capturing atmospheric water vapor dynamics. Key findings include RMSE values of 1.58–2.91 ppm for Tabriz and 2.02–2.16 ppm for Tehran, indicating reasonable agreement between GNSS-derived Nw and radiosonde measurements.

The tomographic model's resolution was optimized to 0.37°–0.5° horizontally and 500–1000 m vertically, with constraints applied to mitigate the ill-posed nature of the inverse problem. The spatial distribution of GNSS rays and the resolution matrix played pivotal roles in achieving reliable reconstructions. Notably, the study underscored the challenges posed by Iran's

uneven radiosonde coverage, emphasizing GNSS tomography as a viable alternative for regions with sparse observational infrastructure.

Future work could explore integrating additional data sources, such as numerical weather models, to refine tomographic accuracy further. The findings contribute to advancing atmospheric monitoring in data-scarce regions, offering practical insights for meteorological applications and climate studies. This research lays the groundwork for expanding GNSS-based tomography in Iran and similar geographically diverse areas, ultimately enhancing weather prediction and environmental monitoring capabilities.

ACKNOWLEDGEMENTS

The authors would like to express their heartfelt gratitude to the organizations and institutions whose support and resources were instrumental in conducting this research. Special thanks are extended to the Iranian National Cartographic Center (NCC) for providing access to the Iranian Permanent GPS Network (IPGN) data, a critical component for the GNSS tomography conducted in this study. Additionally, we deeply appreciate the National Centers for Environmental Information (NCEI) (https://www.ncei.noaa.gov/) for supplying the radiosonde observations utilized in our analyses. The invaluable contributions of these institutions have significantly enriched the quality and depth of this research.

References

Bastin, S., Champollion, C., Bock, O., Drobinski, P., Masson, F., 2007: Diurnal cycle of water vapor as documented by a dense GPS network in a coastal area during ESCOMPTE IOP2. *Journal of Applied Meteorology and Climatology*, *46*(2), 167–182.

Bender, M., Dick, G., Ge, M., Deng, Z., Wickert, J., Kahle, H.-G., Raabe, A., Tetzlaff, G., 2011: Development of a GNSS water vapour tomography system using algebraic reconstruction techniques. *Advances in Space Research*, *47*(10), 1704–1720. https://doi.org/https://doi.org/10.1016/j.asr.2010.05.034

Benevides, P., Catalao, J., Nico, G., Miranda, P. M. A., 2018: 4D wet refractivity estimation in the atmosphere using GNSS tomography initialized by radiosonde and AIRS measurements: results from a 1-week intensive campaign. *GPS Solutions*, *22*(4), 91. https://doi.org/10.1007/s10291-018-0755-5

Bevis, M., Businger, S., Herring, T. A., Rocken, C., Anthes, R. A., Ware, R. H., 1992: GPS meteorology: remote sensing of atmospheric water vapor using the global positioning system. *Journal of Geophysical Research*, *97*(D14), 15787–15801. https://doi.org/10.1029/92jd01517

Brenot, H., Rohm, W., Kačmařík, M., Möller, G., Sá, A., Tondaś, D., Rapant, L., Biondi, R., Manning, T., Champollion, C., 2018: Cross-validation of GPS tomography models and methodological improvements using CORS network. *Atmospheric Measurement Techniques Discussions*, *2018*, 1–42. https://doi.org/10.5194/amt-2018-292

Champollion, C., Masson, F., Bouin, M. N., Walpersdorf, A., Doerflinger, E., Bock, O., Van Baelen, J., 2005: GPS water vapour tomography: Preliminary results from the ESCOMPTE field experiment. *Atmospheric Research*, *74*(1–4), 253–274. https://doi.org/10.1016/j.atmosres.2004.04.003

Couvreux, F., Guichard, F., Redelsperger, J. L., Kiemle, C., Masson, V., Lafore, J. P., Flamant, C., 2005: Water-vapour variability within a convective boundary-layer assessed by large-eddy simulations and IHOP _2002 observations. *Quarterly Journal of the Royal Meteorological Society*, *131*(611), 2665–2693. https://doi.org/10.1256/qj.04.167

de Sá, A., 2019: *Tomographic determination of the spatial distribution of Water Vapour using GNSS observations for real-time applications*. Institute of Geodesy and Geoinformatics.

Elgered, G., Davis, J. L., Herring, T. A., Shapiro, I. I., 1991: Geodesy by radio interferometry: Water vapor radiometry for estimation of the wet delay. *Journal of Geophysical Research: Solid Earth*, *96*(B4), 6541–6555. https://doi.org/https://doi.org/10.1029/90JB00834

Elósegui, P., Ruis, A., Davis, J. L., Ruffini, G., Keihm, S. J., Bürki, B., Kruse, L. P., 1998: An experiment for estimation of the spatial and temporal variations of water vapor using GPS data. *Physics and Chemistry of the Earth*, *23*(1), 125–130. https://doi.org/10.1016/S0079-1946(97)00254-1

Flores, A., LP, G., Elosegui, P., Elgered, G., JL, D., Rius, A., 2000: Sensing atmospheric structure: Tropospheric tomographic results of the small-scale GPS campaign at the Onsala Space Observatory. *Earth, Planets and Space*, *52*(11), 941–945.

Flores, A., Ruffini, G., Rius, A., 2000: 4D tropospheric tomography using GPS slant wet delays. *Annales Geophysicae*, *18*(2), 223–234. https://doi.org/10.1007/s00585-000-0223-7

Forootan, E., Dehvari, M., Farzaneh, S., Karimi, S., 2023: Improving the Wet Refractivity Estimation Using the Extremely Learning Machine (ELM) Technique. *Atmosphere*, *14*(1), 112. https://doi.org/10.3390/ATMOS14010112/S1

Forootan, E., Dehvari, M., Farzaneh, S., Sam Khaniani, A., 2021: A functional modelling approach for reconstructing 3 and 4 dimensional wet refractivity fields in the lower atmosphere using GNSS measurements. *Advances in Space Research*, *68*(10), 4024–4038. https://doi.org/https://doi.org/10.1016/j.asr.2021.08.012

Geng, J., Chen, X., Pan, Y., Mao, S., Li, C., Zhou, J., Zhang, K., 2019: PRIDE PPP-AR: an open-source software for GPS PPP ambiguity resolution. *GPS Solutions*, *23*(4), 1–10. https://doi.org/10.1007/S10291-019-0888-1/METRICS

Gradinarsky, L. P., Jarlemark, P., 2004: Ground-based GPS tomography of water vapor: Analysis of simulated and real data. *Journal of the Meteorological Society of Japan. Ser. II*, *82*(1B), 551–560.

Guerova, G., Jones, J., Douša, J., Dick, G., De Haan, S., Pottiaux, E., Bock, O., Pacione, R., Elgered, G., Vedel, H., Bender, M., 2016: Review of the state of the art and future prospects of the ground-based GNSS meteorology in Europe. *Atmospheric Measurement Techniques*, *9*(11), 5385–5406. https://doi.org/10.5194/amt-9-5385-2016

Guo, J., Yang, F., Shi, J., Xu, C., 2016: An Optimal Weighting Method of Global Positioning System (GPS) Troposphere Tomography. *IEEE Journal of Selected Topics in Applied*

Earth Observations and Remote Sensing, *9*(12), 5880–5887. https://doi.org/10.1109/JSTARS.2016.2546316

Haji-Aghajany, S., 2021: *Function-based troposphere water vapor tomography using GNSS observations*.

Haji-Aghajany, S., Amerian, Y., 2018: Hybrid regularized GPS tropospheric sensing using 3-D ray tracing technique. *IEEE Geoscience and Remote Sensing Letters*, *15*(10), 1475–1479.

Haji-Aghajany, S., Amerian, Y., Amiri-Simkooei, A., 2022: Function-based troposphere tomography technique for optimal downscaling of precipitation. *Remote Sensing*, *14*(11), 2548.

Haji-Aghajany, S., Amerian, Y., Verhagen, S., 2020: B-spline function-based approach for GPS tropospheric tomography. *GPS Solutions*, *24*(3), 88.

Haji-Aghajany, S., Amerian, Y., Verhagen, S., Rohm, W., Schuh, H. (2021: The effect of function-based and voxel-based tropospheric tomography techniques on the GNSS positioning accuracy. *Journal of Geodesy*, *95*(7), 1–17. https://doi.org/10.1007/S00190-021-01528-2/METRICS

Haji-Aghajany, S., Izanlou, S., Tasan, M., Rohm, W., Kryza, M., 2025: High-resolution GNSS troposphere tomography through explainable deep learning-based downscaling framework. *Satellite Navigation*, *6*(1), 22.

Haji Aghajany, S., Amerian, Y., 2017: Three dimensional ray tracing technique for tropospheric water vapor tomography using GPS measurements. *Journal of Atmospheric and Solar-Terrestrial Physics*, *164*, 81–88. https://doi.org/10.1016/j.jastp.2017.08.003

Hanna, N., Trzcina, E., Möller, G., Rohm, W., Weber, R., 2019: Assimilation of GNSS tomography products into the Weather Research and Forecasting model using radio occultation data assimilation operator. *Atmospheric Measurement Techniques*, *12*(9), 4829–4848. https://doi.org/10.5194/amt-12-4829-2019

Heublein, M., Alshawaf, F., Erdnüß, B., Zhu, X. X., Hinz, S., 2019: Compressive sensing reconstruction of 3D wet refractivity based on GNSS and InSAR observations. *Journal of Geodesy*, *93*(2), 197–217. https://doi.org/10.1007/s00190-018-1152-0

Huang, L., Jiang, W., Liu, L., Chen, H., Ye, S., 2019: A new global grid model for the determination of atmospheric weighted mean temperature in GPS precipitable water vapor. *Journal of Geodesy*, *93*(2), 159–176. https://doi.org/10.1007/S00190-018-1148-9/METRICS

Izanlou, S., Amerian, Y., Seyed Mousavi, S. M.: GNSS-DERIVED PRECIPITABLE WATER VAPOR MODELING USING MACHINE LEARNING METHODS, ISPRS Ann. Photogramm. Remote Sens. Spatial Inf. Sci., X-4/W1-2022, 307–313, https://doi.org/10.5194/isprs-annals-X-4-W1-2022-307-2023, 2023.

Izanlou, S., Haji-Aghajany, S., Amerian, Y., 2024: Enhanced Troposphere Tomography: Integration of GNSS and Remote Sensing Data With Optimal Vertical Constraints. *IEEE Journal of Selected Topics in Applied Earth Observations and Remote Sensing*, *17*, 3701–3714. https://doi.org/10.1109/JSTARS.2024.3354884

Jacob, D., 2001: The role of water vapour in the atmosphere. A short overviewfrom a climate modeller's point of view. *Physics and Chemistry of the Earth, Part A: Solid Earth and Geodesy*, *26*(6–8), 523–527. https://doi.org/10.1016/S1464-1895(01)00094-1

Möller, G., 2017: *Reconstruction of 3D wet refractivity fields in the lower atmosphere along bended GNSS signal paths*. Technische Universität Wien.

Nilsson, T., Elgered, G., 2007: Water vapour tomography using GPS phase observations: Results from the ESCOMPTE experiment. *Tellus A: Dynamic Meteorology and Oceanography*, *59*(5), 674–682.

Notarpietro, R., Cucca, M., Gabella, M., Venuti, G., Perona, G., 2011: Tomographic reconstruction of wet and total refractivity fields from GNSS receiver networks. *Advances in Space Research*, *47*(5), 898–912.

Rohm, W., Bosy, J., 2009: Local tomography troposphere model over mountains area. *Atmospheric Research*, *93*(4), 777–783.https://doi.org/https://doi.org/10.1016/j.atmosres.2009.03.013

Rohm, W., Zhang, K., Bosy, J., 2014: Limited constraint, robust Kalman filtering for GNSS troposphere tomography. *Atmospheric Measurement Techniques*, *7*(5), 1475–1486. https://doi.org/10.5194/amt-7-1475-2014

Seeber, G., 2003: *Satellite geodesy*. Walter de gruyter.
Stensrud, D. J. (2009: *Parameterization schemes: keys to understanding numerical weather prediction models*. Cambridge University Press.

Tayfehrostami, A., Amerian, Y., 2025: Analysis of Tropospheric Precipitable Water Vapor Variations Using GNSS Radio Occultation Data and Radiosonde Observations (Case Study: Iran). *Journal of the Earth and Space Physics*. https://doi.org/10.22059/jesphys.2025.396147.1007694

Troller, M. R., 2004: *GPS based determination of the integrated and spatially distributed water vapor in the troposphere*. ETH Zurich.

Trzcina, E., Rohm, W., 2019: Estimation of 3D wet refractivity by tomography, combining GNSS and NWP data: First results from assimilation of wet refractivity into NWP. *Quarterly Journal of the Royal Meteorological Society*, *145*(720), 1034–1051. https://doi.org/https://doi.org/10.1002/qj.3475

Turco, R. P., 1992: Atmospheric chemistry. *Climate System Modeling. Cambridge University Press. New York*, 234–235.

Van Baelen, J., Reverdy, M., Tridon, F., Labbouz, L., Dick, G., Bender, M., Hagen, M., 2011: On the relationship between water vapour field evolution and the life cycle of precipitation systems. *Quarterly Journal of the Royal Meteorological Society*, *137*(S1), 204–223. https://doi.org/https://doi.org/10.1002/qj.785

Yao, Y., Zhao, Q., 2017: A novel, optimized approach of voxel division for water vapor tomography. *Meteorology and Atmospheric Physics*, *129*(1), 57–70. https://doi.org/10.1007/s00703-016-0450-4